Communication

A Broadband Near-Field UHF RFID Reader Antenna With Low Far-Field Gain

Yuan Yao, Yishan Liang, Junsheng Yu, and Xiaodong Chen

***Abstract*— A broadband magnetic coupling antenna with low far-field gain for ultrahigh frequency radio frequency identification near-field applications is presented in this communication. The proposed antenna is consisted of a number of loop units and each unit has in-phase current along the loop. It generates a strong uniformly distributed magnetic field over a large interrogation. To meet different scenarios, the interrogated area can be adjusted by changing the number of units. The proposed antenna has low far-field gain and broadband characteristics. Mechanism analysis is carried out to provide the guidelines for the antenna design. As an example, a 10-unit antenna has been fabricated and measured. The experimental results show that the antenna achieves the impedance matching over the frequency range from 740 to 4600 MHz. And the proposed antenna achieves 100% reading rate with 140 button tags in the region of 100 mm × 750 mm × 12 mm.**

***Index Terms*— Broadband, low far-field gain, near field, radio frequency identification (RFID), reader antenna, ultrahigh frequency (UHF).**

I. Introduction

Recently, passive ultrahigh frequency (UHF) radio frequency identification (RFID) is being applied to the products tracking, supply chain, and bio-sensing applications [1]–[3]. According to the working mechanism, the coupling between reader antennas and tags is divided into magnetic coupling and electrical coupling. The magnetic coupling in near-field applications is more and more attractive because of the capacity of operating in close to metals and liquids [4], [5]. The performance of the RFID is related extremely to reader antenna. The greatest challenge of designing a UHF near-field magnetic coupling reader antenna is to control field distribution. It requires the antenna radiation field concentrated evenly in near field and attenuated rapidly in far field.

The general electrically small loop antennas can only produce a strong and uniform magnetic field in the small central region, because the current features phase-inversion when the perimeter of loop is larger than one wavelength. Some works have been reported to address the design of electrically large loop antennas for UHF near-field applications. To obtain in-phase current along the loop, small capacitances have been introduced in [6]–[8]. Qing *et al*. [9] and Shi *et al*. [10], [11] presented near-field zero-phase shift line loop antennas. However, these single-loop antennas have the characteristic of high far-field gain with omnidirectional radiation and it is probably to misreading the dipole-like tags out of the interrogation zone. Meanwhile, it is required a complex matching network to form the grid array to extend reading area. Another solution to deal with near-field magnetic coupling is based on standing wave structures [12], [13]. The reading area of these antennas can be customized easily. However, the −10 dB impedance bandwidth of those antennas is narrow, the values of which are 15 MHz in [12] and 14 MHz in [13]. They are not enough to cover the whole UHF RFID standard, 860–960 MHz.

In this communication, a broadband low far-field gain antenna for RFID near-field applications is proposed. The proposed antenna is able to provide a strong and uniform magnetic field distribution over a large interrogation zone. The magnetic intensity is attenuated rapidly away from antenna. The measured results show that the antenna matched well from 740 to 4600 MHz. In addition, the reading area is easily customizing to meet different application requirements.

Manuscript received January 8, 2017; revised June 18, 2017; accepted July 9, 2017. Date of publication July 24, 2017; date of current version September 1, 2017. This work was supported by the National Natural Science Foundation of China under Grant 61474122. *(Corresponding author: Yuan Yao.)*

Y. Yao, Y. Liang, and J. Yu are with the Beijing Key Laboratory of Work Safety Intelligent Monitoring, School of Electronic Engineering, Beijing University of Posts and Telecommunications, Beijing 100876, China (e-mail: yaoy@bupt.edu.cn).

X. Chen is with the School of Electronic Engineering and Computer Science, Queen Mary University of London, London E1 4NS, U.K.

Color versions of one or more of the figures in this communication are available online at http://ieeexplore.ieee.org.

Digital Object Identifier 10.1109/TAP.2017.2731375

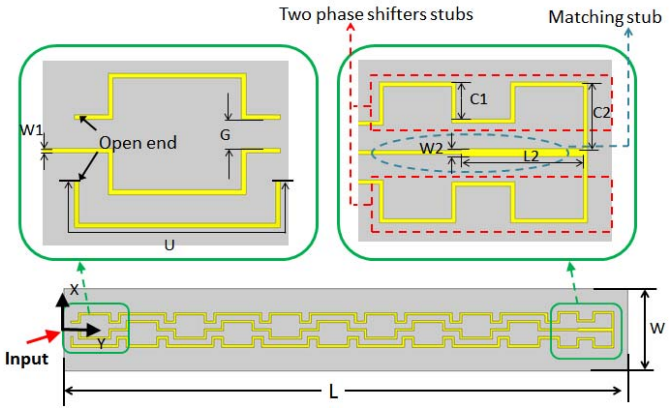

Fig. 1. Configuration of the proposed antenna.

TABLE I
DIMENSIONS OF ANTENNA

L	L2	W	W1	W2	C1	C2	U	G
776	43	120	1.6	3	13.5	24.3	93.5	10

unit: mm

II. Antenna Design and Discussion

A. Antenna Configuration

The proposed antenna can be fabricated onto any substrate and designed with optimizing parameters properly at specific frequency. In this communication, an antenna prototype is fabricated on FR4 substrate with relative dielectric constant of 4.3, and thickness of 1 mm, as shown in Fig. 1. A metal ground is printed on the bottom layer of the substrate and meander microstrip lines are printed on the top. The antenna is comprised of two open-end microstrip lines on two sides and a feeding line in the middle. At the right side of the antenna, there are two phase shifters stubs and a matching stub. Table I lists the optimized dimensions of the proposed antenna. At the input port, the antenna prototype is connected to a 50-Ω SubMiniature version A connector.

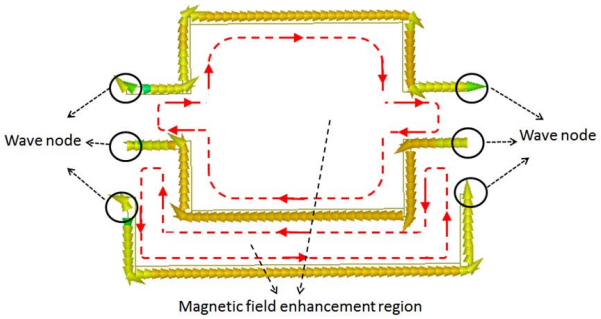

Fig. 2. In-phase loop unit with simulated current distribution at 920 MHz at the phase of 0°.

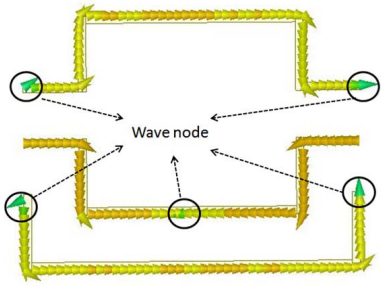

Fig. 3. In-phase loop unit with simulated current distribution at 920 MHz at the phase of 90°.

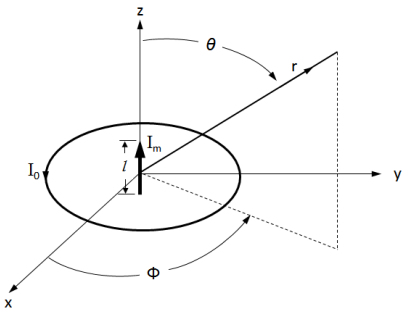

Fig. 4. Geometry for circular loop.

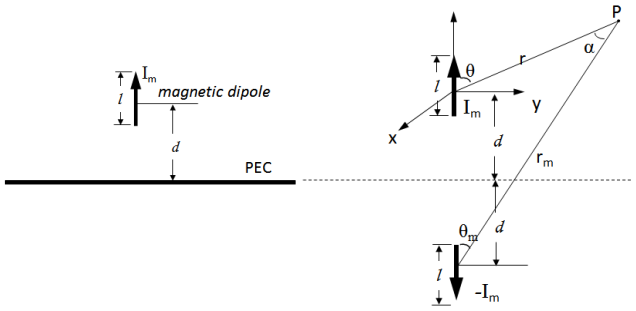

(a) (b)

Fig. 5. (a) Physical arrangement of equivalent source. (b) Distribution of image magnetic dipole.

B. Working Principle of the Antenna

The proposed antenna consists of ten in-phase loop units. The length of each loop unit is approximately equal to $\lambda_g/2$, half operating wavelength on board at frequency 920 MHz. Due to the open end, standing waves are excited on the upper and lower side microstrip lines and the position of the wave node is fixed. The length of phase shifter stubs is also approximately equal to $\lambda_g/2$, which introduce a phase difference of 180° between the upper/lower side microstrip line and the middle microstrip line. The matching stub is adopted to reduce reflection at the branch. The current of the antenna is distributed in 360 phase periods. When the wave node is at the edge of the middle meander line of the unit, we define the phase of 0° at this time. As phase changes, a 90° phase distribution can be obtained. Fig. 2 shows a unit with simulated current distribution at 920 MHz at the phase of 0°. According to the Ampere' law, the magnetic field is enhanced in the central portion as indicated by the dotted line. Meanwhile, the meander units eliminate null zones by bending at the wave node.

Fig. 3 shows the current distribution of a unit at the phase of 90°. It can be seen that in this state the position of the wave node in the middle meander line is changed with phase shifted. The electromagnetic wave excited on the middle line is a kind of transmission mode similar to traveling wave. The middle meander line plays the role of feed and radiation. The electromagnetic waves are fed from the input side and the antenna continuously loses energy due to radiation. So the reflections are minimized and the antenna achieved high return loss in wideband.

C. Analysis of Far-Field Gain

In an actual RFID system, the dipole-like and loop-like tags are always present at the same time in many positions. To avoid misreading other tags, it is necessary to achieve the low far-field gain characteristic for the near-field RFID applications. This section will analyze the far-field characteristic of the proposed antenna. Different from other communications, a ratio coefficient υ is introduced in this section to verify that the field decays more rapidly.

The proposed antenna consists of a number of in-phase loop units. They can be modeled as in-phase loop antennas. To simplify the analysis, consider a small loop antenna. The most convenient geometrical arrangement for the analysis of a small loop antenna is to position the loop symmetrically on the xy plane, at $z = 0$, as shown in Fig. 4. The wire is assumed to be very thin and the current equals I_0, where I_0 is a constant. For analysis purposes, the small loop can be replaced by a small linear magnetic dipole along the z-axis with constant current I_m. In such a case, the magnetic field components can be written as H_{or}, $H_{o\theta}$, $H_{o\Phi}$ [14].

In the proposed antenna, the in-phase loop unit has a dielectric structure having a ground plate formed on one surface thereof. The boundary condition is different from identical small loop, which changes the field distribution in free space.

According to method of images [15], the field distribution can be calculated directly by set up appropriate equivalent source. As shown in Fig. 5, a vertical magnetic dipole located at a distance d above a large grounded conducting plane can be equivalent to two opposite vertical magnetic dipoles without ground. The conduct ground is assumed to be very large and the loss is ignored. In Fig. 5(b), the radiated fields of any position(r, θ, Φ) $(0° \le \theta \le 90°)$ except at the origin are given by as

$$H_{\mathrm{pr}} = H_{\mathrm{or}} + H_{\mathrm{mr}}\cos(\alpha) + H_{m\theta}\sin(\alpha) \quad (1)$$

$$H_{p\theta} = H_{o\theta} + H_{m\theta}\cos(\alpha) - H_{\mathrm{mr}}\sin(\alpha) \quad (2)$$

where H_{mr}, $H_{m\theta}$ are image magnetic dipole radiated fields.

In this communication, a ratio coefficient $\upsilon(r, \theta, \Phi)$ is defined as the radio of magnitude of total magnetic field in a given position from the antenna to the identical magnetic dipole magnitude of total

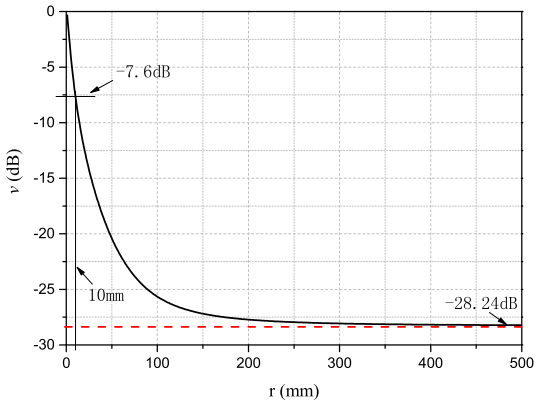

Fig. 6. Coefficient υ at $\theta = 0°$ with respect to r.

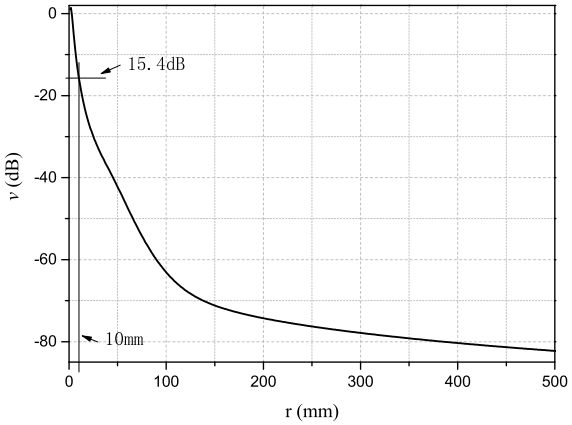

Fig. 7. Coefficient υ at $\theta = 90°$ with respect to r.

magnetic field. In mathematical form, it is expressed as

$$\upsilon(r, \theta, \Phi) = \sqrt{\frac{|H_{\mathrm{pr}}|^2 + |H_{p\theta}|^2 + |H_{p\phi}|^2}{|H_{\mathrm{or}}|^2 + |H_{o\theta}|^2 + |H_{o\phi}|^2}}. \tag{3}$$

The coefficient υ means the value of magnetic intensity attenuation. The expression for $\upsilon(r, \theta, \Phi)$ to decibels (dB) is

$$\upsilon(\mathrm{dB}) = 20 \log_{10}(\upsilon). \tag{4}$$

To demonstrate this analysis, an example is considered here. The thickness of the proposed antenna's substrate is 1 mm, which means $d = 1$ mm. And the operating frequency is set at 920 MHz to plot coefficient υin Figs. 6 and 7. The radiated fields are symmetrical about Φ. So whatever value it takes, the result is unaffected.

In the region very close to the antenna (kr $\ll$ 1), the magnetic intensity will be inversely proportional to r^3. And in the far field (kr $\gg$ 1), it will be inversely proportional to r. As shown in Fig. 6, the value of υ decays rapidly with r increasing. In the near field, the magnetic intensity is weakened but it can still activate the tags in this region. However, the magnetic intensity is weakened greatly in the far field and it is too weak to activate the tags.

By the same way, the value of υ at $\theta = 90°$ is given in Fig. 7. Different from the vertical direction, the υ reduced more rapidly and it is approximately equal to zero in far field. Thus£the antenna has a characteristic that the magnetic field is concentrated in the interrogation zone and attenuated rapidly at edge.

The proposed antenna consists of a number of low far-field gain in-phase loop units. Thus, it has low gain characteristic in far field.

Actually, the small loop wire assumed to be very thin is not very accurate. Because the dimensions of the microstrip line are finite

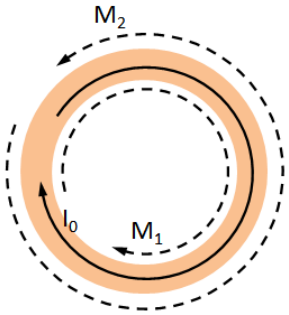

Fig. 8. Equivalent magnetic current distribution of a microstrip loop.

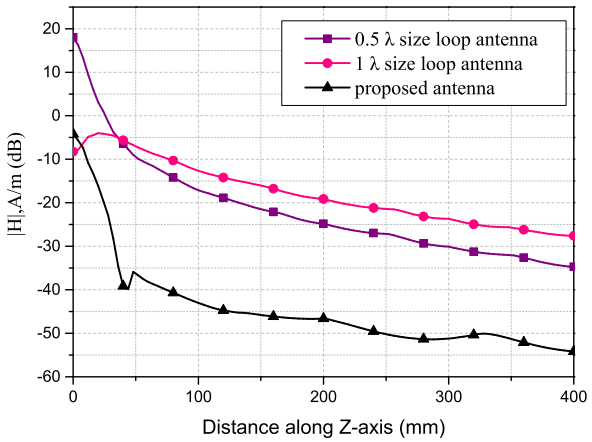

Fig. 9. Simulated magnitude of magnetic field with respect to distance in different size loop antennas.

along the width, the fields at the edges of the line undergo fringing. As illustrated in Fig. 8, the slots of microstrip line can be equivalent to a pair of reversal magnetic currents M_1, M_2. Similar to the above analysis, it will cancel each other in the far-field region. And in the near field, it is not the main radiator that can be neglected.

For better show the field attenuation characteristic of the proposed antenna. Two general loop antennas in perimeter of 0.5λ and 1λ were simulated by HFSS software. All the antennas were placed symmetrically on the xy plane, at $z = 0$. Fig. 9 showed the simulated strength of H-field in the center of different antennas with respect to distance along z-axis.

It can be seen that the 0.5λ size loop antenna with in-phase current distribution generate the strongest magnetic field intensity in the near field. And the magnetic fields of 1λ size loop antenna were canceled in the near field due to the presence of the reversal current. As expected, the H-fields of proposed antenna were weakened greatly in the far field.

It has been illustrated that the far-zone field of antenna array is equal to the product of the field of a single element and the array factor. That is

$$H(\mathrm{total}) = [H(\mathrm{single\ element})] \times [\mathrm{array\ factor}]. \tag{5}$$

In this expression, [H (single element)] can be calculated by (1) and (2). However, the conduct ground is not infinite large and the correction factor σ is introduced here

$$I_m = \sigma I_0. \tag{6}$$

In the calculation, the correction factor σ is 0.94. To simplify the theoretical model, [array factor] is assumed that ten elements have identical amplitudes with in-phase in λ/4 separation. And then, the calculated and simulated gain patterns are plotted in Fig. 10.

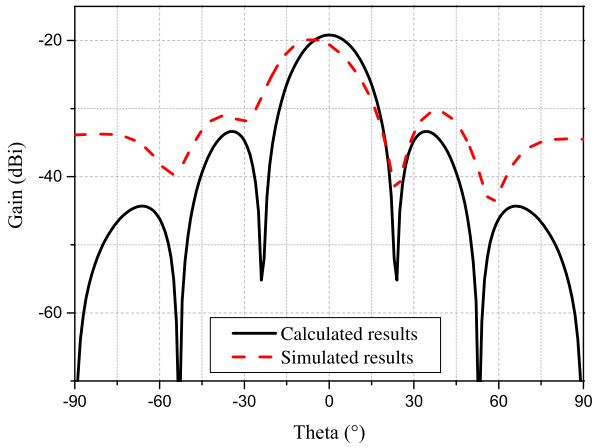

Fig. 10. Gain patterns of calculated and simulated in 920 MHz.

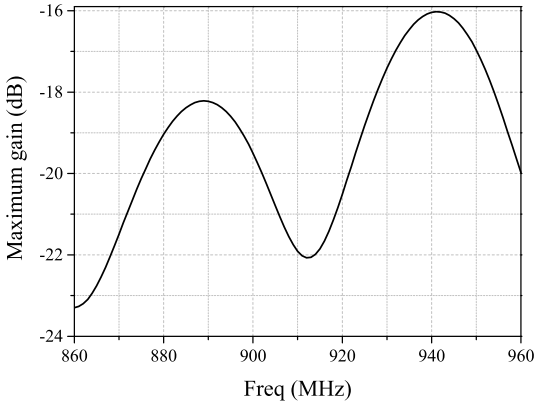

Fig. 11. Simulated maximum gain of the proposed antenna.

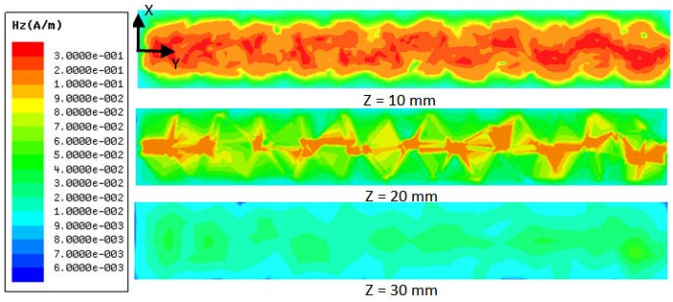

Fig. 12. Simulated magnetic field component H_Z distributions at 920 MHz in the horizontal plane of the antenna at $z = 10$, 20, 30 mm.

It can be seen that the simulated maximum far-field gain close to the theoretical value.

In order to verify the analysis above, the simulated far-field maximum gain of the proposed antenna is shown in Fig. 11. It can be seen that the peak gain is below -16 dBi from 860 to 960 MHz (UHF band), which verifies the proposed antenna is feasible to the near-field applications.

D. Magnetic Field Distribution

Based on the microstrip structure, the proposed antenna has directional radiation characteristic. As shown in Fig. 12, the magnetic field component H_Z is concentrated and evenly distributed above the antenna. As the distance from the antenna surface increases, the magnetic field strength gradually decreases. Meanwhile, the field strength decay rapidly at the edge. This field distribution allows the antenna to read tags in the interrogation zone only and to avoid misreading tags out of the interrogation zone.

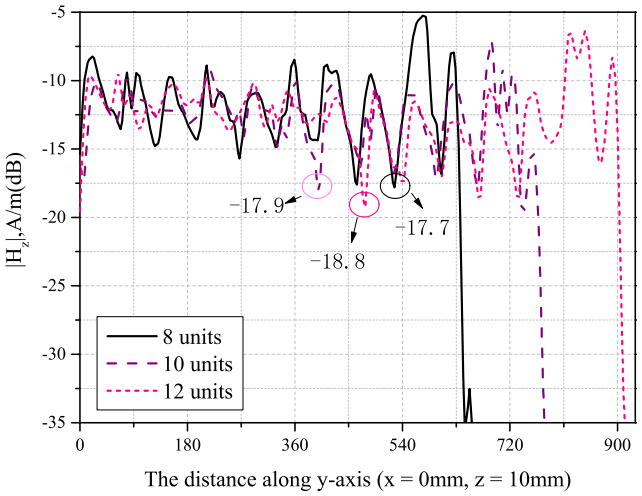

Fig. 13. Simulated magnetic field distributions at $x = 0$ mm, $z = 10$ mm in different number of units.

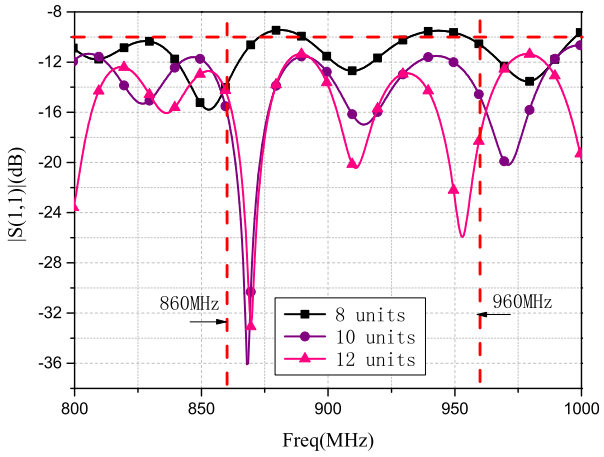

Fig. 14. Simulated $|S_{11}|$ in different number of units.

The establishment of the coordinate system is the same as Fig. 1. Fig. 13 illustrates simulated magnetic field distributions along y-axis at the $x = 0$ mm and 10-mm distance from antenna surface at 920 MHz. The different curves represent magnetic field intensity of the antenna with different number of units. It can be seen that the interrogation zone becomes larger when the units increase. The proposed 10-unit antenna achieves a uniform magnetic field distribution with a maximum variation of 10 dB in the interrogation zone. However, the dimension of a loop-like tag is usually longer than 10 mm which is leaped over the minimum magnetic field intensity. According to energy conservation law, the field intensity is weakened in the interrogation zone as the number of unit increasing. From simulated results, the minimum value of the magnetic field intensity is attenuated when the antenna prototype increasing. In practice, the upper limit of the number of units can be calculated according to this criterion and the sensitivity of the tags.

E. Simulated Impedance Matching

Fig. 14 shows the simulated reflection coefficient curves for different number of units. It can be seen that the impedance matched well

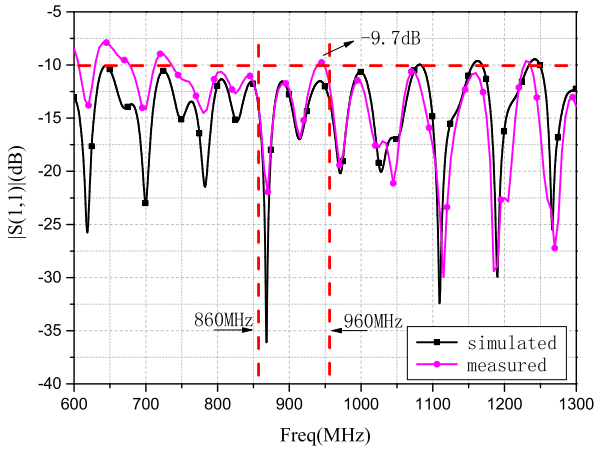

Fig. 15. Simulated and measured $|S_{11}|$ of the proposed antenna.

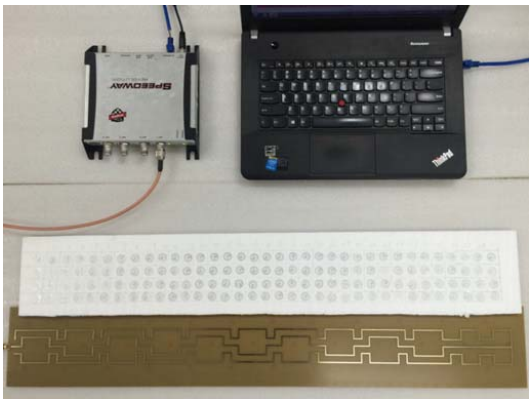

Fig. 16. Near-field measurement setup using the Impinj Speedway R420 and the proposed antenna prototype with 140 tags.

within UHF RFID working frequency band from 860 to 960 MHz. As the number of units increasing, the maximum of $|S_{11}|$ is reduced. The simulation results validate the principle of broadband.

III. Measurement Results

In order to verify the design concept and simulation results, the antenna prototype is implemented onto a piece of FR4 substrate with size of 776 mm × 120 mm × 1 mm and it is measured in an open environment.

A. Simulated and Measured Impedance Matching

The impedance matching measurement of the proposed antenna has been carried out using Agilent 8753ES vector network analyzer. The simulated and measured $|S_{11}|$ of the proposed 10-unit antenna are shown in Fig. 15. A good agreement between simulation and measurement results is obtained. It can be seen that the $|S_{11}|$ less than −10 dB ranges from 860 to 960 MHz except at 945 MHz is −9.7 dB. Although open-end terminated at the antenna, the $|S_{11}|$ of which has a nature of traveling wave and it has lots of fluctuations. The slight deviation of $|S_{11}|$ is believed to be caused by the instability of FR4 substrate and fabrication error.

In order to view the impedance matching characteristic of the antenna more, higher frequencies $|S_{11}|$ of the proposed 10-unit antenna have been measured. The measured results show that $|S_{11}|$ is less than −9 dB up to 4600 MHz.

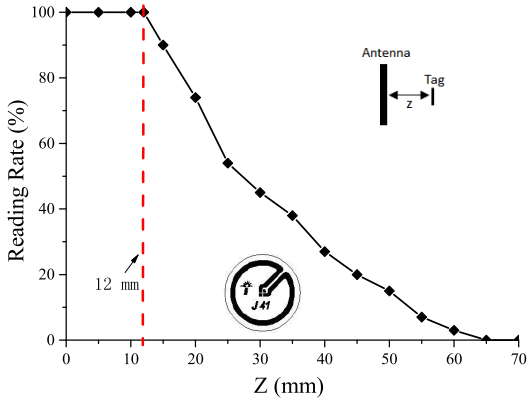

Fig. 17. Measured reading rate with respect to reading distances.

B. Reading Range

To further test the performance of the proposed antenna, the antenna prototype has been used as the reader antenna in the UHF RFID system to simultaneously detect 140 button type tags (Impinj J41, 12 mm × 12 mm) [16].

Fig. 16 demonstrates the test configuration, where the proposed antenna is connected to an Impinj Speedway R420 reader with 30 dBm output power operating at Chinese RFID bands, 920–925 MHz. A dimension of 100 mm × 750 mm × 5 mm foam sheet is placed horizontally above the antenna surface. The sheet is divided equally into 140 grids with size of 20 mm × 20 mm and each grid attaches a J41 tag (the diameter of J41 is 12 mm). The read sensitivity of J41 tag is −19.5 dBm, the tag chip of which is Impinj Monza 4. In the vertical direction, the foam sheet is moved with a gap of 5 mm and it records detected tags number at every moved gap.

We repeat the test ten times and take average. The detected number divided by the total number is reading rate. The reading rate against the reading distances is exhibited in Fig. 17. A 100% reading rate is achieved within a maximum distance of 12 mm, which means the reading range of the proposed antenna is 100 mm × 750 mm × 12 mm.

IV. Conclusion

This communication presents a broadband low far-field gain antenna for RFID near-field applications. The proposed antenna has the advantages of simple structure, low cost, and easy processing. The antenna configuration, working principle, simulated, and measured results have been presented and discussed. It achieves a 100% reading rate with 140 tags at the distances up to 12 mm from the antenna surface. It is easy to customize the interrogation area by adjusting the number of meander line units. We expect that those features of the proposed antenna will be useful for near-field RFID applications.

References

[1] K. Jaakkola, "Small on-metal UHF RFID transponder with long read range," *IEEE Trans. Antennas Propag.*, vol. 64, no. 11, pp. 4859–4867, Nov. 2016.

[2] J. Lorenzo, A. Lázaro, R. Villarino, and D. Girbau, "Modulated frequency selective surfaces for wearable RFID and sensor applications," *IEEE Trans. Antennas Propag.*, vol. 64, no. 10, pp. 4447–4456, Oct. 2016.

[3] J.-M. Lin and Z.-Q. Hou, "Bio-sensing and monitor system design with micro array probes on an active RFID tag," in *Proc. Int. Nanoelectron. Conf.*, Jan. 2010, pp. 346–347.

[4] S. Amendola, S. Milici, and G. Marrocco, "Performance of epidermal RFID dual-loop tag and on-skin retuning," *IEEE Trans. Antennas Propag.*, vol. 63, no. 8, pp. 3672–3680, Aug. 2015.

[5] J. M. Laheurte, S. Protat, and A. Louzir, "Performance analysis of UHF RFID tags dedicated to power supply cords," *IEEE Trans. Antennas Propag.*, vol. 63, no. 11, pp. 5241–5245, Nov. 2015.

[6] D. M. Dobkin, S. M. Weigand, and N. Lye, "Segmented magnetic antennas for near-field UHF RFID," *Microw. J.*, vol. 50, no. 6, pp. 1–7, Jun. 2007.

[7] X. Qing, Z. N. Chen, and C. K. Goh, "UHF near-field RFID reader antenna with capacitive couplers," *Electron. Lett.*, vol. 46, no. 24, pp. 1591–1592, Nov. 2010.

[8] Y. S. Ong, X. Qing, C. K. Goh, and Z. N. Chen, "A segmented loop antenna for UHF near-field RFID," in *Proc. IEEE Antennas Propag. Soc. Int. Symp. (APSURSI)*, Jul. 2010, pp. 1–4.

[9] X. M. Qing, C. K. Goh, and Z. N. Chen, "A broadband UHF near-field RFID antenna," *IEEE Trans. Antennas Propag.*, vol. 58, no. 12, pp. 3829–3838, Dec. 2010.

[10] J. Shi, X. Qing, Z. N. Chen, and C. K. Goh, "Electrically large dual-loop antenna for UHF near-field RFID reader," *IEEE Trans. Antennas Propag.*, vol. 61, no. 3, pp. 1019–1025, Mar. 2013.

[11] J. Shi, X. Qing, and Z. N. Chen, "Electrically large zero-phase-shift line grid-array UHF near-field RFID reader antenna," *IEEE Trans. Antennas Propag.*, vol. 62, no. 4, pp. 2201–2208, Apr. 2014.

[12] Y. Yao, C. Cui, J. Yu, and X. Chen, "A meander line UHF RFID reader antenna for near-field applications," *IEEE Trans. Antennas Propag.*, vol. 65, no. 1, pp. 82–91, Jan. 2017.

[13] Y. Liang, Y. Yao, J. Yu, and X. Chen, "Design of a novel meander line reader antenna for UHF near-field RFID," in *Proc. 11th Int. Symp. Antennas, Propag. EM Theory*, Oct. 2016, pp. 19–21.

[14] C. A. Balanis, *Antenna Theory: Analysis and Design*. Hoboken, NJ, USA: Wiley, 2005, pp. 237–238.

[15] D. K. Cheng, *Field and Wave Electromagnetics*. Beijing, China: Tsinghua Univ. Press, 2007, pp. 159–161.

[16] *RFID Tags*. Accessed on Apr. 2017. [Online]. Available: http://www.impinj.com